Quantum Dot DNA Bioconjugates: Attachment Chemistry Strongly Influences the Resulting Composite Architecture

Kelly Boeneman,[†,¶] Jeffrey R. Deschamps,[†,¶] Susan Buckhout-White,[†,⊥] Duane E. Prasuhn,[†] Juan B. Blanco-Canosa,[∥] Philip E. Dawson,[∥] Michael H. Stewart,[‡] Kimihiro Susumu,[‡] Ellen R. Goldman,[†] Mario Ancona,[§] and Igor L. Medintz[†,*]

[†]Center for Bio/Molecular Science and Engineering, Code 6900, [‡]Optical Sciences Division, Code 5611, and [§]Electronic Science and Technology Division, Code 6876, U.S. Naval Research Laboratory, Washington D.C. 20375, United States, [⊥]George Mason University, 4400 University Drive, Fairfax, Virginia 22030, United States, and [∥]Departments of Cell Biology and Chemistry, The Scripps Research Institute, La Jolla, California 92037, United States. [¶]These authors contributed equally to this work.

ABSTRACT The unique properties provided by hybrid semiconductor quantum dot (QD) bioconjugates continue to stimulate interest for many applications ranging from biosensing to energy harvesting. Understanding both the structure and function of these composite materials is an important component in their development. Here, we compare the architecture that results from using two common self-assembly chemistries to attach DNA to QDs. DNA modified to display either a terminal biotin or an oligohistidine peptidyl sequence was assembled to streptavidin/amphiphilic polymer- or PEG-functionalized QDs, respectively. A series of complementary acceptor dye-labeled DNA were hybridized to different positions on the DNA in each QD configuration and the separation distances between the QD donor and each dye-acceptor probed with Förster resonance energy transfer (FRET). The polyhistidine self-assembly yielded QD—DNA bioconjugates where predicted and experimental separation distances matched reasonably well. Although displaying efficient FRET, data from QD—DNA bioconjugates assembled using biotin—streptavidin chemistry did not match any predicted separation distances. Modeling based upon known QD and DNA structures along with the linkage chemistry and FRET-derived distances was used to simulate each QD—DNA structure and provide insight into the underlying architecture. Although displaying some rotational freedom, the DNA modified with the polyhistidine assembles to the QD with its structure extended out from the QD—PEG surface as predicted. In contrast, the random orientation of streptavidin on the QD surface resulted in DNA with a wide variety of possible orientations relative to the QD which cannot be controlled during assembly. These results suggest that if a particular QD biocomposite structure is desired, for example, random *versus* oriented, the type of bioconjugation chemistry utilized will be a key influencing factor.

KEYWORDS: semiconductor nanocrystal · quantum dot · self-assembly · biotin · streptavidin · DNA · FRET · Förster resonance energy transfer · dye · fluorophore · modeling · structure

The use of nanoparticle (NP) biocomposite materials continues to grow in myriad applications ranging from *in vivo* imaging to molecular electronics.[1−3] Chemistries which controllably interface biologicals including proteins, peptides, and DNA with the NP materials are a key part of developing this technology. Ideally, such chemistries would allow attachment of the biological with control over final ratio or valence per NP, separation distance from the NP, orientation on the NP, and affinity for the NP.[4,5] Several different attachment strategies are commonly used; however, almost all provide only limited access to these desirable properties. The most common approach targets groups commonly found on the biological for linkage to those present or that can be easily introduced onto the NP surface. For example, carbodiimide (EDC) chemistry forms an amide bond between carboxyls and amines; these groups are both ubiquitous to proteins and easily introduced onto NP surfaces.[6] Another frequently used attachment exploits the high binding affinity of biotin−avidin, with the requisite groups introduced onto either component.[6,7] Less common, although highly promising, are the families of bioorthogonal chemistries which introduce unique functional groups onto both the NP and biological to facilitate specific reactions while not altering native groups already present. These are typified by the superfamily of "click" and chemoselective ligation chemistries.[8−10] Regardless of the chemical approach used, understanding the structures that arise when assembling NP bioconjugates and the effects this has on subsequent function is integral to their development.

Our work has focused on developing luminescent semiconductor nanocrystal or quantum dot (QD) bioconjugates for a variety of biosensing and molecular imaging applications. Their unique quantum-confined optical properties have made QDs particularly useful as both fluorophores

*Address correspondence to igor.medintz@nrl.navy.mil.

Received for review August 24, 2010 and accepted November 01, 2010.

Published online November 17, 2010.
10.1021/nn1021346

and Förster resonance energy transfer (FRET) donors or acceptors.[11−16] Bioconjugates made with QD materials can be considered prototypical examples of the chemistry issues facing most NP composites as a variety of different attachment strategies are currently utilized in their assembly. For these purposes, we focus specifically on chemistries for joining DNA to QDs as a model system. This attachment is most commonly accomplished using four different approaches: (1) EDC coupling chemistry to join amine or carboxyl-functionalized DNA to the cognate groups present on the QD surface.[17−19] (2) Direct attachment of DNA to QDs by thiol bonding. To accomplish this, DNA is obtained with a terminal thiol modification, reduced, and allowed to coordinate to the QD shell *via* dative thiol interactions similar to the chemistry used for cap exchange with bifunctional charged or polyethylene glycol (PEG)/thiolated solubilizing ligands.[17−19] (3) Polyhistidine peptide−DNA assembly to QD surfaces. We, and others, have shown that terminally modifying DNA with a polyhistidine (His_n) sequence can allow its rapid self-assembly to the QDs *via* metal-affinity coordination in a manner analogous to that used for protein and peptide purification with nitrilotriacetic acid-chelated divalent cations.[20−23] (4) Biotinylated DNA attachment to streptavidin-coated QDs. For this, DNA is obtained with a terminal biotin modification and allowed to interact directly with streptavidin QDs, which are most often obtained commercially.[17−19]

In this report, we compare the composite structures that arise when DNA is attached to QDs using the latter two chemistries. DNA modified with either a terminal biotin or a His_n sequence were assembled to streptavidin or PEG-functionalized QDs, respectively. Complementary dye-labeled DNAs were hybridized to different positions on the DNA in each QD configuration and QD−dye donor−acceptor separation distances were probed with FRET. The resulting distances were compared to theoretical predictions based upon implicit assumptions about how the DNA assembles to the QDs.

RESULTS AND DISCUSSION

DNA Sequences, Acceptor Dye Placement, and Spectral Overlap. The goal of this work was to utilize FRET to investigate how attachment chemistry can affect subsequent QD−DNA conjugate architecture. To accomplish this, three different constructs were assembled: construct 1, a dye-only DNA control assembly; construct 2, peptide-modified DNA self-assembled to PEGylated QDs; construct 3, biotin-modified DNA linked to streptavidin-coated QDs. To maintain consistency, each construct utilized the same DNA sequences, acceptor dye placements, and overall configuration (see Figure 1A). The 40 base pair (bp) backbone DNA sequence is designed to be hybridized with a series of four sequential complementary single-stranded (ss) sequences, denoted A−D. These can be either unlabeled spacer (sp) segments or prelabeled with dyes at their 5′ ends as indicated. This allows acceptor dyes to be placed at a series of increasing 10 bp increments from a terminally located donor dye or from the QD when the DNA is attached. Backbone DNA was obtained with either a 3′ amine or a 3′ biotin insertion (Figure 1A). The final dsDNA sequence used here originates from Ouchi and satisfies structural criteria such as:[24] the duplex DNA structure is rigid and not influenced by intramolecular H-bonding; the chromophore labeling sites are located every 10 residues (∼33 Å), placing them all on the same side of the DNA duplex and separating them by one helical turn; and A−T pairs are placed near the chromophores to avoid guanine-induced quenching.[24] In agreement with the work of Protozanova and structural modeling (see Supporting Information Figure S-1), the nicks in the DNA arising from the use of the multiple complementary hybridized sequences have a minimal effect on the rigidity of the overall dsDNA structure.[25]

QD−DNA constructs are formed following the hybridization of individual segments to 40-mer backbone DNAs. To form the peptide-linked QD construct, we utilize self-assembly facilitated by the metal-affinity coordination of polyhistidine $(His)_n$ sequences. This interaction occurs between the imidazolium side chain groups on oligohistidine sequences and the Zn-rich surface of CdSe/ZnS core/shell QDs.[20] We, and others, have demonstrated that a variety of QDs can be self-assembled with proteins and peptides expressing clearly available $(His)_n$ sequences in a rapid manner (<30 min) due to the high-affinity equilibrium binding constants of this solution interaction ($K_d \sim 1$ nM).[20,21,26−29] Importantly, control can be exercised over the ratio or valence of molecules assembled per QD through the molar equivalents utilized. We have previously shown that DNA sequences terminally modified with $(His)_n$-peptidyl sequences can also self-assemble to QDs in the same manner.[21,30] Here, we exploit aniline-catalyzed hydrazone ligation chemistry to join the modified backbone DNA to a $(His)_6$-peptidyl sequence (Figure 1B). The Dawson lab has shown that this coupling reaction is characterized by enhanced bioconjugation rates of 10^1-10^3 M^{-1} s^{-1} in mild, aqueous conditions (slightly acidic to neutral pH) and can reach equilibrium ($K_{eq} = 2.3 \times 10^6$ M^{-1}) in under 30 min using 100 mM aniline catalyst with 10 μM of reactants.[22,31] The single primary amine on the backbone DNA was first derivatized to a benzaldehyde and then chemoselectively ligated to the HYNIC-modified $(His)_6$-peptide sequence in the presence of aniline, as detailed in the Materials and Methods section (Figure 1B). The biotin/streptavidin-linked QD construct was formed through self-assembly of biotin-terminated backbone DNA to the as-purchased streptavidin QDs.

Figure 1C shows the absorption and emission spectra of the various QDs and dyes used in this study. Table

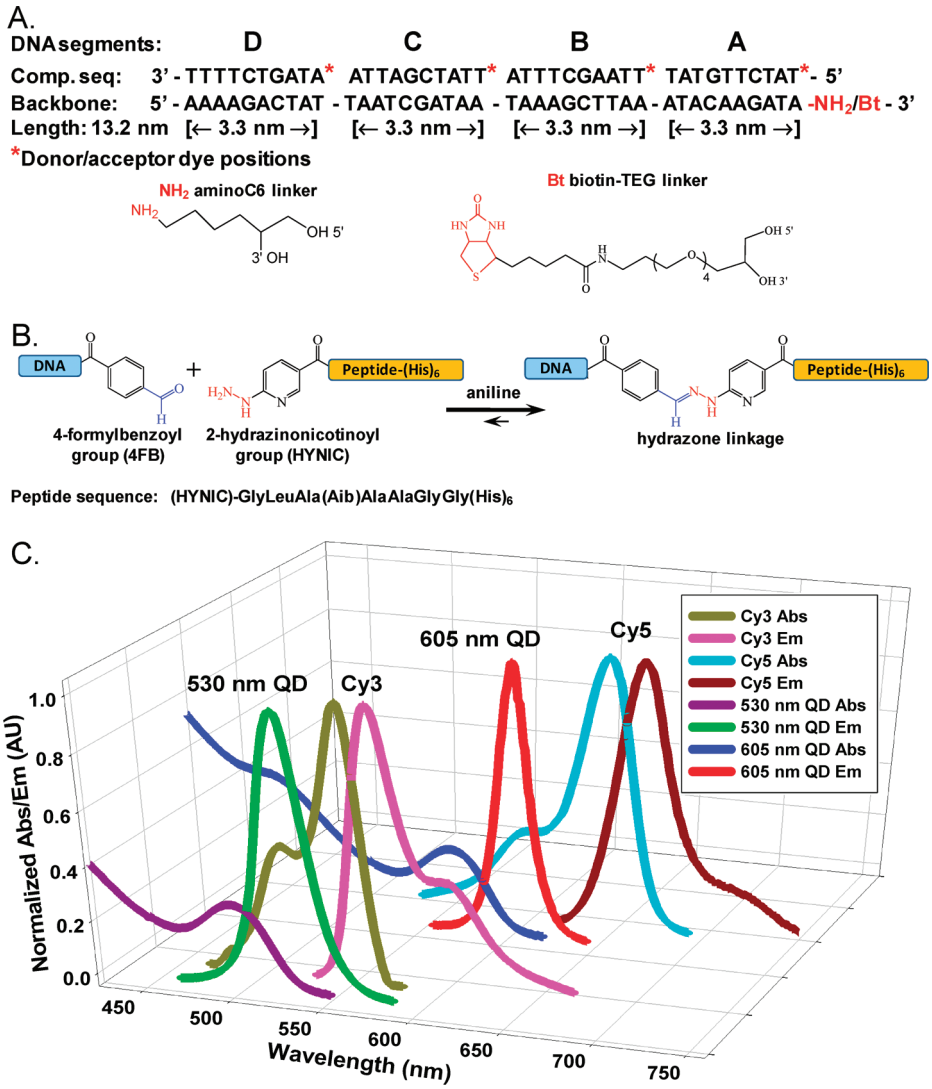

Figure 1. DNA sequences, chemoselective ligation, and spectral overlap. (A) Sequences of the DNA backbone with a 3′ amino or biotin functionalization and the complementary DNA segments (A−D) showing donor/acceptor labeling sites at the 5′ end of each. (B) Aniline-catalyzed hydrazone ligation between the aldehyde (blue) of the 4FB group and the peptidyl HYNIC group (red) used to link DNA to the $(His)_6$-peptide. (C) Plot showing the spectral overlap of the fluorophore donor−acceptor species used; Cy3−Cy5, 530 nm QD−Cy3, and 605 nm QD−Cy5.

1 presents the relevant photophysical properties including the Förster distances or R_0 values along with the spectral overlap function $J(\lambda)$. These were derived by treating the QD or each dye as a single donor interacting individually with each dye acceptor.[32] Depending on the degree of spectral overlap and the acceptor extinction coefficient, the R_0 values range from 53 Å for the Cy3−Cy5 donor−acceptor pair to ~75 Å for the 605 nm QD−Cy5 pair. The large value of the latter arises from a combination of the QDs high quantum yield of ~70% and the large Cy5 acceptor molar extinction coefficient of 250 000 M^{-1} cm^{-1} (Table 1). The repeated ~33 Å periodicity of dye attachment points across the final 132 Å dsDNA structure (Figure 1) in conjunction with the calculated R_0 values suggests that decreasing FRET efficiencies should be expected when increasing the donor−acceptor separation distances between terminal donors and dyes located at sequential positions A−D.

TABLE 1. Photophysical Properties of the QDs and Fluorophores Used.

fluorophores	quantum yield	extinction coefficient (M^{-1} cm^{-1})	λ_{max} absorption	λ_{max} emission	R_0 in Å with Cy3 $J(\lambda)$	R_0 in Å with Cy5 $J(\lambda)$
530 nm QD	0.20	640000 (at 350 nm)		530 nm	54 (6.67×10^{-13})[b]	
605 nm QD	0.70	580000 (at 532 nm)		605 nm		75 (1.37×10^{-12})
Cy3	0.14[a]	150000	550 nm	570 nm		53 (8.51×10^{-13})
Cy5	0.27[a]	250000	649 nm	670 nm		

[a]Determined from dye-labeled DNA segments. [b]Spectral overlap function in units of cm^3 M^{-1}.

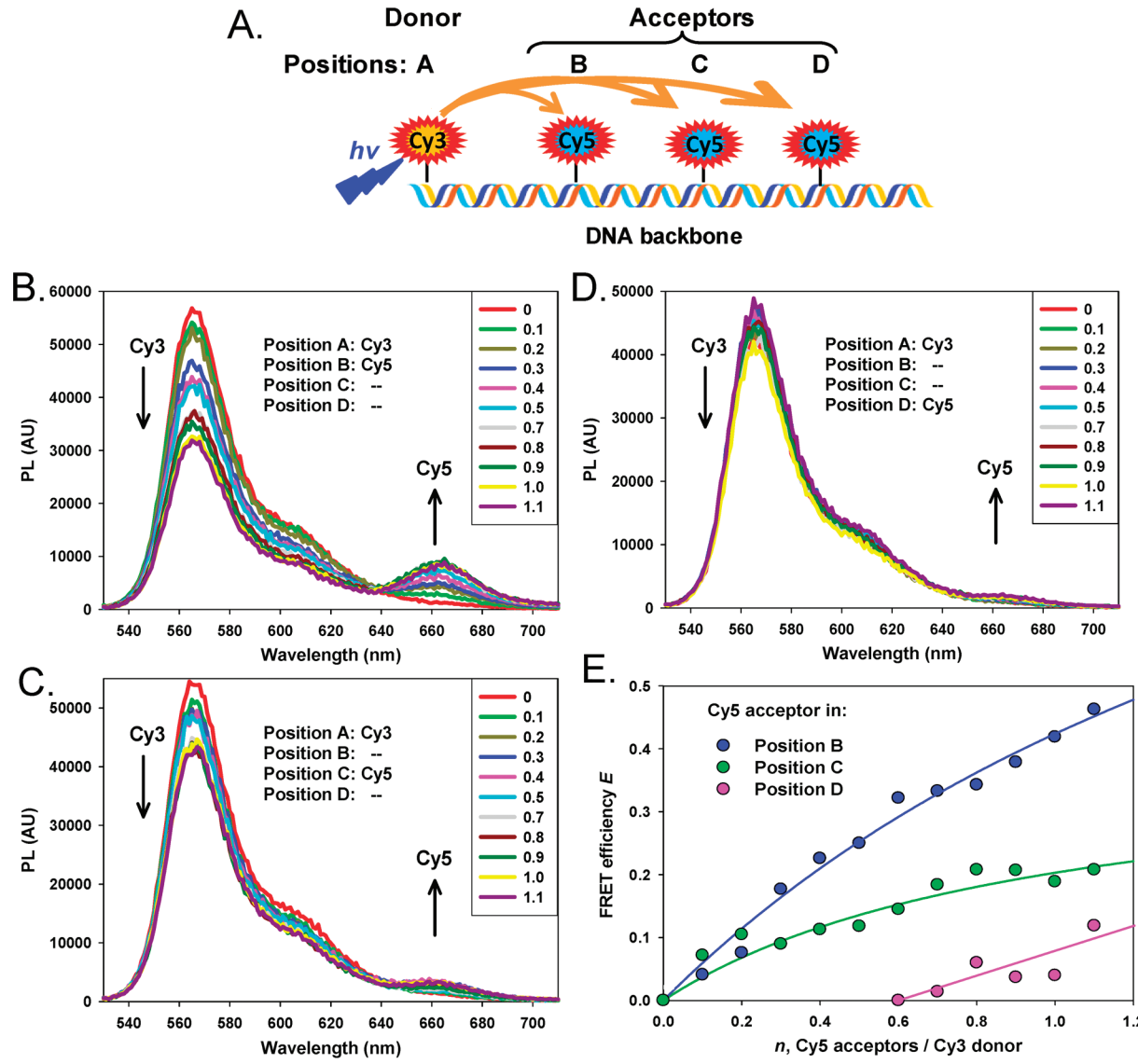

Figure 2. Construct 1: dye-based DNA assembly. (A) Schematic of the nanoconstruct composed of a Cy3 donor at position A with a Cy5 acceptor placed at position B, C, or D. When a position is not used, the equivalent unlabeled spacer is hybridized in that location. (B–D) PL spectra of Cy3 donor in position A with increasing molar ratios of Cy5-labeled acceptor DNA placed in positions B, C, or D. (E) FRET efficiency *E* for each acceptor position *versus* acceptor valence. Lines of best fit added.

Construct 1: Dye-Only DNA Control Assembly. We began by examining the FRET interactions of dyes attached at increasing separation distances within just the DNA structure itself (see Figure 2A). Here, a Cy3-labeled donor DNA is hybridized in position A while Cy5-labeled acceptor DNA is sequentially alternated between positions B, C, and D with the remaining positions filled with unlabeled sp strands. Figure 2B–D shows representative composite spectra collected from each configuration as the discrete ratio of Cy5 acceptor dye is systematically increased while the Cy3 donor in position A remains fixed at ~1 per construct. For each position to be interrogated, Cy5-labeled and unlabeled sp strands were precombined in different molar ratios to increase the fractional amount of Cy5 acceptor per Cy3 donor from 0 to ~1 incrementally. The mixing of labeled and unlabeled DNA to achieve a constant ratio relative to the backbone keeps the structure rigid, while varying the discrete acceptor number alters the donor–acceptor ratio pairing. FRET efficiency *E* for each configuration as calculated from Cy3 donor PL loss is plotted in Figure 2E. See Supporting Information Figure S-3 for plots comparing the FRET *E* and Cy5 acceptor sensitization in these configurations. In comparing the data, several processes become readily apparent. First, the rate of FRET increases concomitant to increases in the ratio of dye acceptor per donor especially at the closest putative separation distances of Cy3 in position A and Cy5 in B. In Figure 2B, the Cy3 donor PL drops ~50% at a donor/acceptor ratio of 1, while Cy5 sensitization increases and appears to plateau at ~15%. As Cy3 donor/Cy5 acceptor separation distance increases, the rate of FRET drops substantially, as again verified by Cy3 donor PL loss and Cy5 sensitization. For

TABLE 2. Donor−Acceptor Separation Distances

donor	acceptor	acceptor position	predicted[a] r (Å)	measured[b] r (Å)
Cy3[c]	Cy5	B	30 ± 20	49
		C	66 ± 20	62
		D	93 ± 20	88[d]
530 nm QD	Cy3	A	68 ± 10	67
(His_6 metal affinity)		B	99 ± 10	72[e]
		C	129 ± 10	86[e]
		D	153 ± 10	114[f]
605 nm QD	Cy5	A	146 ± 10	99
(streptavidin−biotin)		B	173 ± 10	112
		C	208 ± 10	103
		D	236 ± 10	103

[a]Derived as described in the Materials and Methods section; value accounts for the rotational freedom provided by the dye attachment linkers. For the Cy3−Cy5 system, the −20 Å value accounts for rotation of both dye linkers. [b]Estimated using eqs 2−4. [c]Cy3 donor in position A. [d]Value of r is derived from three highest acceptor ratio efficiencies. [e]Derived from where FRET E plateaus. [f]Derived from four highest acceptor efficiencies. 530 nm QD radius = 28 Å, 605 nm QD radius = 75 Å (excludes streptavidin).

example, in Figure 2C, placing the Cy5 an additional 10 bp further away at position C decreases the maximum E to ~20% while Cy5 sensitization concomitantly drops to ≤5%. Lastly, moving the acceptor to position D decreases E to a maximum of ≤10% with Cy5 sensitization becoming almost negligible. Adding more DNA acceptors above a ratio of 1 to each configuration slightly increased the FRET E (data not shown). However, this subsequent increase could be fitted with a linear Stern−Volmer function indicative of solution-phase diffusional quenching interactions.[32] This was expected because the QD−DNA constructs were fully hybridized.

Table 2 lists the separation distances r derived from analyzing this data set along with predicted separation values. The latter were estimated using the dsDNA length and incorporate the dye's freedom of rotation. Both donor and acceptor dyes are attached to the DNA *via* a 3-carbon linker and phosphate bond. This linker, combined with the relative size of these somewhat linear dyes (structures in Supporting Information Figure S-2), provides for quite a large freedom of rotational movement. As such, we assign an estimated error of ±20 Å to each predicted separation distance to account for conformations where both dyes (±10 Å per dye) are either oriented close to each other or, alternatively, as far as possible from each other. This, in essence, estimates the separation minima and maxima. This is slightly less than twice the theoretical maximal 14.6 Å (29.2 Å) extension possible for this structure and represents a more conservative, energetically favorable range. For these purposes, we recognize that it is highly unlikely that the dye linker will assume and maintain a fully extended end-to-end conformation. Without any rotational freedom, the dye separation distances should closely track the 10 bp periodicity of ~33 Å. Measured distances deviate somewhat from the predicted values, although these still increase sequentially and fall within ranges that include the predicted rotational freedom. The largest deviation is seen at the closest positioning (A to B) with 49 Å measured *versus* the predicted 30 ± 20 Å. Measured values for the other two separation distances demonstrate better agreement with predicted values (62 *vs* 66 Å and 88 *vs* 93 Å for A to C and A to D placements, respectively) and show <10% deviation. We speculate that at the closest A to B positioning, some donor−acceptor dye pairs within the overall ensemble may prefer orientations that place them as far as possible from each other (steric repulsion), as reflected by the large separation distance. Alternatively, given the linearity of cyanine dye structure, their extended lengths can also place them at distances shorter than 30 Å, where the point dipole approximation may break down. More importantly, these results confirm that the dsDNA construct is relatively rigid and that sequentially increasing relative donor−acceptor separation alters energy transfer efficiency in a manner consistent with Förster predictions. This can be observed with data originating from the largest separation distance (positions A−D). Comparing the Cy3−Cy5 R_0 of 53 Å with the estimated separation distance approaching 100 Å (~2 × R_0) predicts an efficiency of ≤10% which is indeed observed.

Construct 2: Peptide-Modified DNA Self-Assembled to PEGylated QDs. Confident in the DNA's structural rigidity, we proceeded to attach the dsDNA to the QDs (see Figure 3A). In this context, the QD acts as a central donor/nanoscaffold that is self-assembled with increasing ratios of surrounding dye-labeled dsDNA. The Cy3 dye acceptor position was then systematically varied from position A to D within the DNA with each configuration assessed by FRET. Figure 3B−E shows representative composite spectra collected from each configuration as the ratio of dye-labeled DNA self-assembled per QD was increased. Figure 3F plots the corresponding FRET E for each acceptor position as calculated from QD donor PL loss. When the FRET data is examined, several processes again become apparent. FRET E increases in a manner that follows the valence of acceptor dyes arrayed around the QD. This is most apparent at the closest putative separation of QD with Cy3 in position A. As shown in Figure 3B, the QD PL drops more than 80% while Cy3 sensitization increases dramatically as the ratio of acceptor is increased from 0 to 8. Further, as QD donor/Cy3 acceptor separation distance increases with sequential placement, the rate of FRET drops dramatically. In the closest configuration (Cy3 in position A), FRET E appears to plateau at around 80% for a nominal ratio of 8 dye-labeled DNA per QD while the corresponding Cy3-sensitized emission approaches nearly 40% (Supporting Information Figure S-4B). Observed FRET E then systematically decreases in a manner that tracks position relative to the QD donor. The largest predicted separation distance should be achieved when

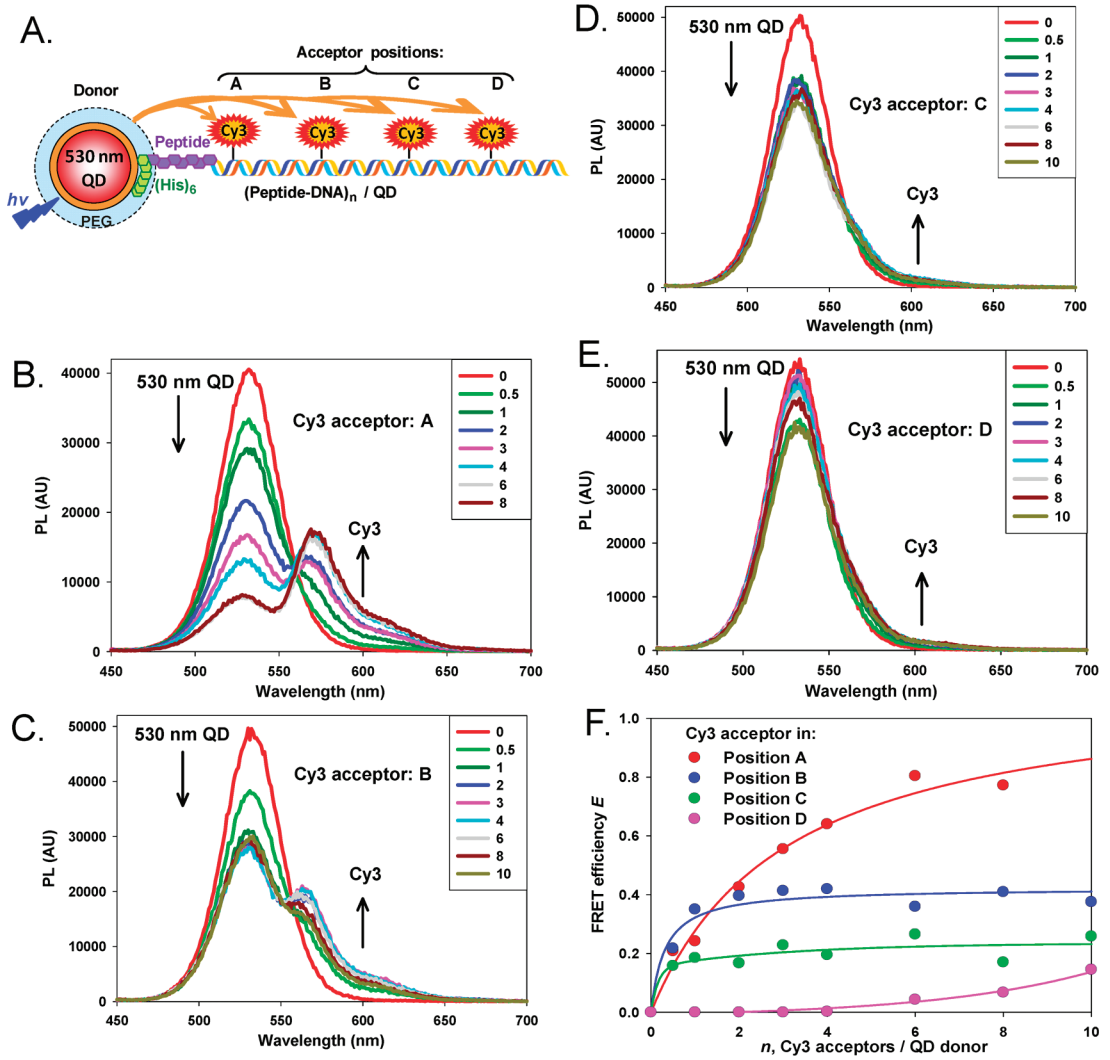

Figure 3. Construct 2: $(His)_6$-peptide−DNA QD assembly. (A) Schematic of the nanoconstruct composed of a 530 nm QD donor self-assembled with $(His)_6$-labeled peptide DNA and Cy3 acceptors placed at positions A−D. When a position is not used, the equivalent unlabeled spacer is hybridized in that location. (B−E) PL spectra of QD donors self-assembled with increasing molar ratios of Cy3-labeled DNA in positions A−D, respectively. (F) Plot of FRET efficiency *E* for each acceptor position *versus* acceptor valence. Lines of best fit added.

Cy3 acceptor is placed at terminal position D, and indeed, observed FRET *E* is insignificant for <5 acceptors per QD; this only increases to ~10% when the acceptor number is brought up to a valence of 10 with no corresponding Cy3 sensitization observed. We note an interesting FRET response when Cy3 acceptor is placed in positions B and C. Rather than increase in proportion to acceptor ratio (as when in position A and D), FRET *E* increases to a discrete value at ratios of ~2 and then remains relatively constant. For these data, distances were estimated from the first few points until the plateau is reached. Despite this, the overall maximum FRET *E* is quite distinct for each acceptor position (~0.4 and ~0.2 for positions B and C, respectively) and falls where expected between the data collected for acceptor in positions A and D. We partially ascribe this behavior to the dsDNA structure's freedom of movement relative to the QD surface, discussed below (see Modeling and Figure 5A).

QD donor to Cy3 acceptor center-to-center separation distances derived from analyzing the data in each configuration along with predicted separation values are given in Table 2. In each case, the predicted separation distances assume the DNA extending out perpendicular from the QD and accounts for the QD core/shell radius of ~28 Å (assuming 4−5 monolayers of ZnS),[33] the $(His)_6$ portion of the peptide directly attached to the QD along with a further portion laterally extending away from the QD surface (~20 Å), the HYNIC group amino C6 linker portion (~15 Å, see Figure 1), and the DNA extension to each acceptor position. The dye acceptor's rotational freedom is again represented by an estimate of ±10 Å. Comparing predicted *versus* derived distances shows a good match for the smallest separation distance (68 *vs* 67 Å for QD to Cy3 in position A); these are essentially the same value. Importantly, the measured separation distances do increase systematically when Cy3 is moved sequentially from positions A

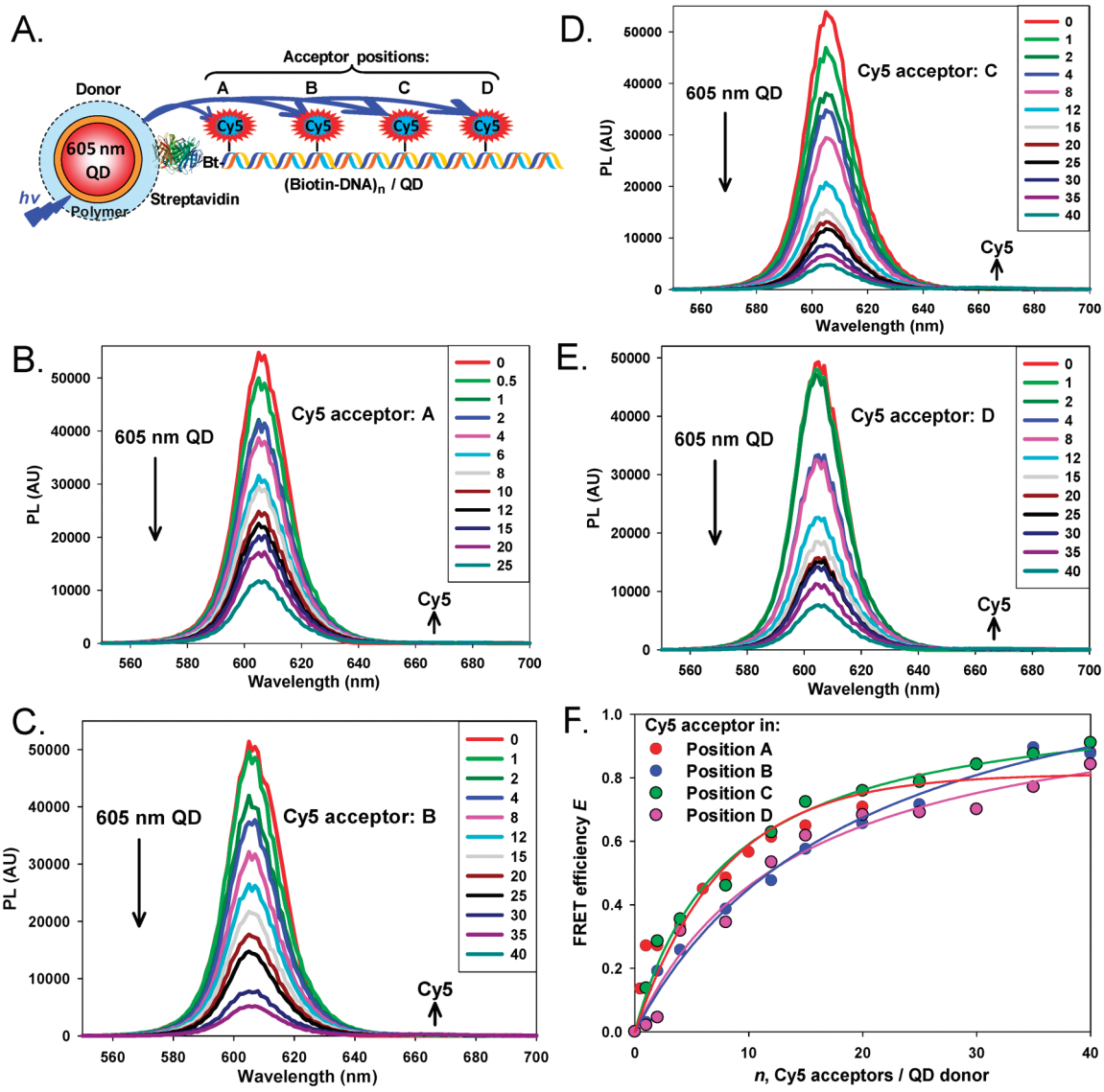

Figure 4. Construct 3: biotin−DNA streptavidin QD assembly. (A) Schematic of the nanoconstruct composed of a streptavidin-functionalized 605 nm QD bound to the biotin-labeled 5′ end of the DNA backbone hybridized with Cy5 acceptor DNA at positions A−D. When a position is not used, unlabeled spacer DNA is hybridized in that location. (B−E) PL spectra of 605 nm QD donors conjugated to increasing molar ratios of Cy5-labeled DNA in positions A−D, respectively. (F) Plot of FRET efficiency *E* for each acceptor position *versus* acceptor valence. Lines of best fit added.

to D, although the measured values for acceptor positions C and D are smaller than those predicted. The largest distance measured of 114 Å approaches 75% of the predicted 153 Å span for the end-to-end DNA separation length. The other discrepancies between observed and predicted distances range from 27 Å for position B to 43 Å for position C. We again ascribe these differences to the dsDNA structure's freedom of movement relative to the QD surface, discussed below (see Modeling and Figure 5A).

Construct 3: Biotin-Modified DNA Linked to Streptavidin-Coated QDs. The last construct investigated utilized the same DNA sequences; however, Cy5 dye was substituted as the acceptor here for spectral overlap with the 605 nm streptavidin QD donor emission. These QDs were utilized as they are perhaps the most common type of streptavidin-functionalized nanocrystal used in FRET studies. In this case, the DNA backbone was obtained with a 3′ biotin modification on a tetraethylene glycol (TEG) linker for attachment to the QDs (see Figure 4A). The TEG facilitates biotin binding to streptavidin's relatively deep binding pocket. Cy5-labeled acceptor DNAs were hybridized onto the biotinylated backbone DNA in positions A−D, and the final dsDNA construct was allowed to attach to the QD *via* biotin−streptavidin interactions as described. Figure 4B−E shows representative composite spectra collected from each construct as the ratio of dye-labeled DNA assembled per QD was increased. The valence of acceptor DNA per QD was increased to a maximum of 25 or 40 to allow for saturation given the predicted average ratio of 5−10 streptavidin/QD from the manufac-

turer's specifications and assuming 2−3 sterically available binding sites per protein. Figure 4F plots the corresponding FRET *E* for each construct/acceptor position as calculated from QD donor PL loss. Several differences between this data set and the previous two are immediately apparent. QD donor PL loss is again quite dramatic and directly tracks the corresponding increase in acceptor valence in each construct. Loss plateaus at around a valence of 20−30/QD with a FRET *E* that approaches 80%. Compared to the DNA-only assemblies in construct 1, negligible Cy5 acceptor sensitization is noted for each construct here; however, this was not unexpected. Although an excellent FRET quencher, minimal Cy5 acceptor sensitization from a variety of QD donors has been noted previously.[30,34,35] More importantly, QD donor PL loss and the corresponding FRET *E* appear to be identical regardless of which position the acceptor dye is hybridized to on the DNA sequence relative to the QD (see Figure 4F).

Comparing the 605 nm QD donor to Cy5 acceptor center-to-center separation distances *versus* those predicted for these assemblies in Table 2 shows how stark these differences are. The predicted values again assume the DNA extending out perpendicular from the QD surface and account for the increased QD core/shell/polymer size along with that of the streptavidin and its rotation around the Cy5 attachment linker (±10 Å). Although predicted separation values increase from 146 to 236 Å, measured values are actually centered on an 18 Å range around 97−115 Å (average 104.5 ± 7.6 Å). Control experiments where equivalent amounts of Cy5 dye alone, DNA assemblies lacking the biotin function, biotin or biotinylated unlabeled DNA were exposed to the same QDs resulted in negligible FRET at almost all ratios along with no visible changes to the QD PL (data not shown). The 605 nm QD donors used here are also known to have a slightly elongated shape; however, the aspect ratio is not significant enough to account for the different efficiencies observed between materials.

Modeling. We utilized modeling (described in Materials and Methods) to simulate the QD−DNA structures and to provide insight into the somewhat disparate FRET-based distances we observe in these two QD nanoassemblies. Figure 5A shows a structural model of construct 2, the $(His)_6$-peptide-modified DNA as self-assembled to 530 nm PEGylated QDs. The core/shell QD is represented by the blue sphere of radius ~27−28 Å, and the PEG solubilizing layer is simulated by the surrounding crimson crown of ~30 Å.[33] The latter are assumed to be in an energy-minimized state rather than fully extended. The $(His)_6$ are shown interacting directly with the QD surface as previously determined.[20] A yellow ribbon is used to represent the α-helical portion of the peptide and to delineate the $(His)_6$ from the HYNIC linker portion. Individual DNA strands within the dsDNA structure are highlighted in orange and yellow, and the estimated maximal rotational extension for each dye molecule as attached to each DNA segment is simulated by the magenta spheres. Two orientations of the DNA relative to the QDs are highlighted in the figure. In conformation *i*, the DNA is placed extending directly outward from the QD surface and the dye locations correspond to the maximal separation values predicted in Table 2. In conformation *ii*, the DNA is adjusted to account for each of the measured *r* values derived from FRET with an emphasis on the data from positions A and D. The dashed lines represent expected or measured distances within each configuration. The tilting of the structure relative to the QD surface in the latter conformation may represent the combined influence of peptide structure, the peptide−DNA linkage, and peptide−DNA−PEG interactions. The PEG layer serves to keep the peptide portion relatively rigid and extending away from the QD surface, and the DNA is also relatively rigid due to its double-stranded structure. We surmise that there is rotational freedom or flexibility around the point where the DNA is attached to the peptide; this most likely corresponds to the C6-alkane portion of the amino linker at the DNA's terminus which lies near the outer boundary of the PEG layer. This allows the rigid DNA the ability to rotate around its axis closest to the QD and assume many different conformations relative to the QD surface. In more simplistic terms, the rigid DNA rotates around the peptide−DNA linkage which functions as a pivot point. This is also located near the outer edge of the surrounding PEG layer. As we utilize FRET to interrogate this system, the closest dye approaches to the QD donor dominate the measured efficiencies although they also help define the closest approach of the DNA structure relative to the QD which is the structure depicted here. The surrounding PEG layer probably prevents any closer approach of the rigid dsDNA to the QD surface. We speculate that this complex interaction may be responsible for the plateau of FRET *E* observed for the dyes in positions B and C. However, when Cy3 acceptor is placed in position D, it is now so distant from the QD that FRET is not seen until much higher ratios are used.

The structures shown in Figure 5B simulate construct 3, the biotinylated DNA as bound to the 605 nm streptavidin QDs. In this case, a ~75 Å radius sphere is used to simulate the combined QD core/shell and polymer coating. The streptavidin protein is shown in orange with DNA attached at all four binding sites. Again, maximal rotational extension for each dye molecule when present on each individual DNA segment is simulated by the magenta spheres. A key assumption made in assembling this structure is that the streptavidin is randomly attached to the QD surface. This linkage is most likely accomplished with EDC or similar active ester coupling chemistry as stipulated by the manufacturer and should result in 2−3 available binding sites per protein, although all four are occupied in the model.

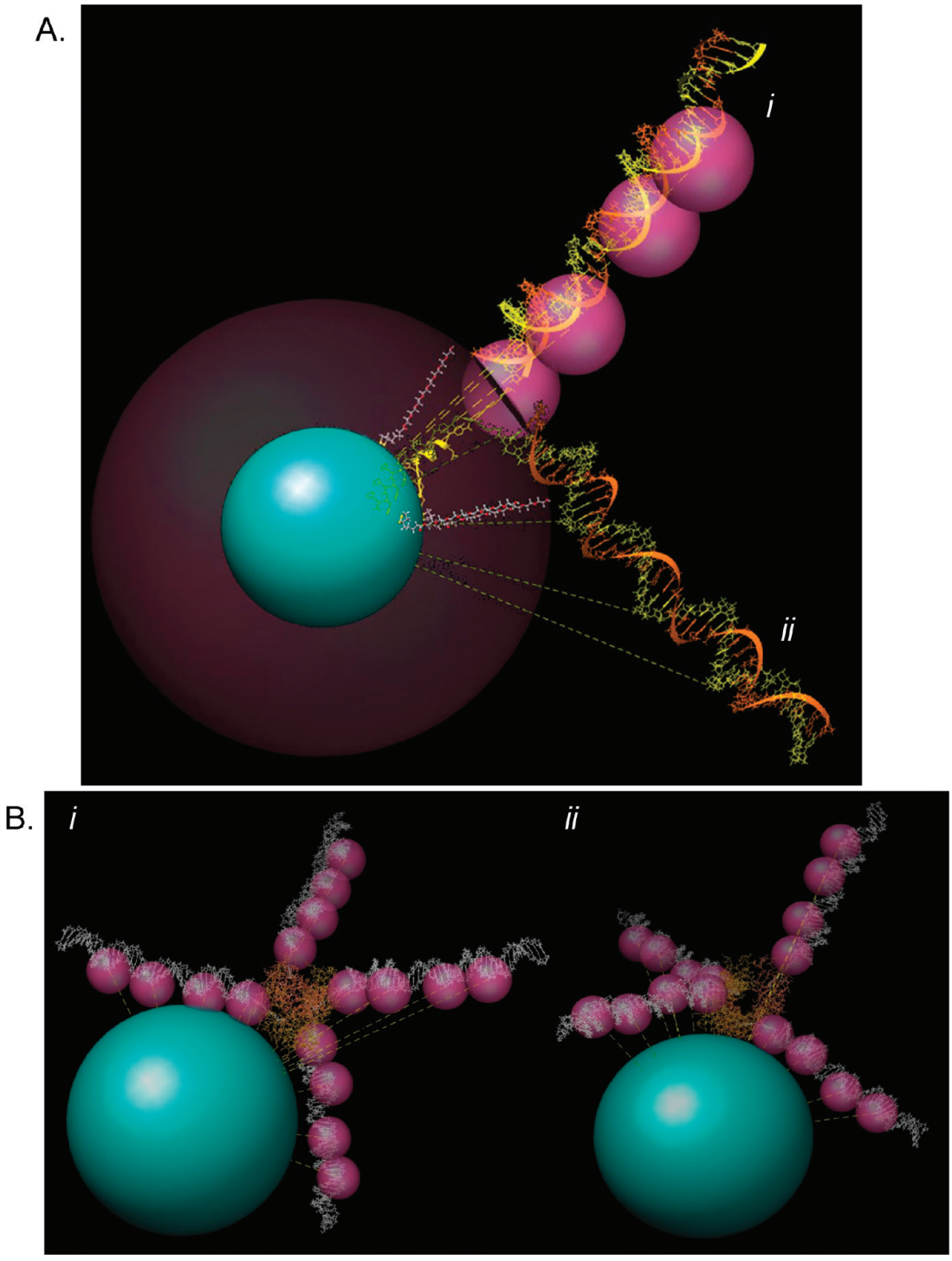

Figure 5. Modeling of QD−DNA structures. (A) $(His)_6$-peptide−DNA bound to 530 nm QDs. The QD is shown as the central blue sphere with a radius of 27−28 Å.[33] The DHLA-PEG ligand is indicated by the crimson halo with an estimated extension of 30 Å utilized here for modeling purposes. DHLA−PEG ligands in an energy-minimized conformation are shown within the crimson sphere. The $(His)_6$ portion of the peptide is shown with a yellow ribbon attached to the HYNIC linker. Individual DNA strands within the dsDNA structure are shown in orange and yellow. The rotational extension of the dye molecules are shown by the magenta spheres. Two possible orientations of the DNA relative to the QDs are shown. (*i*) DNA extending linearly outward from the QD surface and (*ii*) DNA adjusted for the measured *r* values. Dashed lines represent expected or measured distances for each configuration. (B) Biotinylated DNA bound to the 605 nm streptavidin QDs. The QD core/shell/polymer is simulated by a blue sphere of ~75 Å radius according to manufacturer specifications. The streptavidin is shown in orange with DNAs (white) attached at all four binding sites. Fluorescent extensions of the dye molecules are shown by the magenta spheres. Two possible orientations of the DNA relative to the QDs are shown and are derived by changing the orientation of the streptavidin relative to the QD surface. Note that regardless of orientation, several dyes at all possible acceptor sites (A−D) are always in close proximity to the QD surface.

Two possible orientations of the DNA relative to the QDs are shown and are derived by simply rotating the orientation of the streptavidin relative to the QD surface. A third conformational would orient one of the binding sites such that it is in contact with or oriented toward the QD surface, thus reducing the maximum number of binding sites to three (data not shown).

This simulated structure strongly suggests that, given an ensemble of QDs displaying a heterogeneous mixture of multiple streptavidin orientations and binding sites, the biotinylated DNA will also always be bound to the QDs in many random orientations. More importantly, we see that, within these conformations, even when reorienting the dyes among all possible acceptor sites on the DNA (A−D), some dyes are always in close proximity or tangential to the QD surface. Thus, similar FRET efficiencies should be obtained regardless of hybridized DNA acceptor positioning; this directly matches experimentally obtained results. Despite the large QD donor−dye acceptor separation distance intrinsic to using these polymer-coated QDs in conjunction with the dsDNA persistence length of ~100 Å DNA, relatively efficient FRET should also be observed at higher acceptor ratios within the conjugates given this close orientation and the large R_0 value of 75 Å, and this also matches experimental results. Indeed, FRET efficiencies between 50 and 60% are consistently obtained at acceptor valences of ≤15 per QD (Figure 4F). Given streptavidin's deep binding pocket, there may be less freedom of DNA rotation once bound to the QD−protein conjugate; however, this should not alter the observed FRET significantly. We recognize that the measured distances that are utilized in constructing this model may be biased toward the low side as more efficient FRET configurations dominate any collected signal. Although this might account for some of the differences between modeled and measured distances, these fluctuations cannot account for the drastic difference between experimental and predicted distances within this construct. The static model utilized here is meant to provide a means to visualize the differences in structure that we postulate and is not meant to be a simulation that accounts for all possible orientations.

CONCLUSIONS

Due to its facile nature, there are many examples where dye-labeled/biotinylated DNA has been attached to streptavidin-coated QDs and utilized for single-molecule, molecular beacon, aptamer, and other forms of FRET-based sensing.[34−44] Some implicit assumptions have been made when using QD constructs assembled with this chemistry, and most significant among them is that the dye acceptors on the DNA will be located at a uniform set of centrosymmetric distances from the central QD. Indeed, many of these same reports have derived donor−acceptor separation distances for their QD conjugates from the FRET data.[34,35,38−41]

In this report, we utilize FRET to probe the separation distances within QD conjugates as we sequentially move acceptor position along a dsDNA attached to the central QD *via* two common assembly chemistries. This approach is a derivative of a technique we previously utilized to determine the orientation of a protein self-assembled on a QD.[45] There, multiple residues within maltose binding protein were site-specifically labeled with an acceptor dye and the different FRET-derived distances measured from the central QD to each acceptor site on the attached protein, providing a best-fit solution for protein−QD orientation. The experimental approach used here confirms that QD−DNA conjugates assembled using His_n metal-affinity coordination have structures with the DNA extending out somewhat radially from the QD surface within an area that most probably is defined and limited by some freedom of lateral movement. We find evidence for a quasi-uniform set of increasingly longer separation distances between the central QD and the surrounding dye acceptor(s). Although there are some discrepancies, the FRET efficiency is generally found to be dependent upon the ratio of dye acceptors per QD donor and separation distances. The steric repulsion resulting from the surrounding layer of PEGylated QD surface ligands probably contributes significantly to the DNA's orientation relative to the QD in the final structure. This is a gratifying result as we frequently measure FRET-based distances within QD−peptide or DNA structures assembled with His_n chemistry and in some cases have also incorporated these data into models of the conjugates which were assembled to provide similar insight into structure/function relationships.[30,46]

For assemblies constituted using biotin−streptavidin interactions, we also find FRET to be quite efficient and directly dependent upon the number of acceptors attached to the QDs similar to the above reports. This suggests that these constructs should be valid for simple types of signal transduction and biosensing, for example, monitoring the presence or absence of protease activity or aptamer binding to target. However, in contrast to the above results, within this construct, we find that the FRET efficiency does not depend upon the assumption of a discrete set of donor−acceptor separation distances being present. The data derived here in conjunction with structural modeling strongly suggest that the derived distances represent an average of all possible acceptor positions. Additionally, given the multiple streptavidin binding sites, there is no control over where individual biotin acceptors interact. Attempting to reduce the number of binding sites by titrating in free biotin would still not control where any acceptor DNA complex bound. As FRET is directly dependent upon donor−acceptor separation, the dye acceptors binding closest to the QD surface will induce the highest energy transfer and always

dominate the resulting ensemble signal. This would preclude estimating intra-assembly QD donor/dye acceptor separation distances when using this attachment chemistry. Analyzing data utilizing these conjugates for single-molecule FRET sensing or quantitative analysis may also be significantly complicated by this heterogeneity. We surmise that similar issues may be applicable to QD dye acceptor structures assembled with biotinylated peptides or other types of linking moieties.[47,48] It should be noted that, due to its proprietary nature, we did not investigate the role, if any, that the QDs' polymer coating may exert upon the conformation of attached surface DNA. We also did not consider steric hindrance caused by placing the streptavidins in close proximity to each other on the QDs surface.

More sophisticated QD-FRET-based conjugates are continually being developed for a variety of biosensing applications, and it is predicted that these will also soon start to transition to live cell and *in vivo* utility.[11,29,49,50] Control over intraconjugate architecture will be key to the function of these composite materials and will directly depend upon the assembly chemistries utilized. Clearly, known and controlled orientation of biomolecules in the QD conjugates will be the preferred approach in most cases. The results presented here strongly suggest that this may not be feasible when using common attachment chemistries such as biotin−streptavidin. It is probable that similar structural heterogeneity issues are applicable to a variety of other bioconjugates assembled from different types of NP materials and biologicals.[7,51,52] Expanding the available "toolbox" of NP bioconjugation chemistries with a focus on those that provide controlled assemblies[4] along with developing sophisticated techniques for analyzing their structure−function relationship can help address these issues and improve the future design of such composite materials.

MATERIALS AND METHODS

Quantum Dots. The 530 nm emitting CdSe/ZnS core/shell QDs were synthesized using a standard high-temperature reaction of organometallic precursors in hot coordinating solvents.[33,53] These QDs were made soluble in aqueous media through exchange of the native capping shell with dihydrolipoic acid (DHLA) appended with methoxy-terminated polyethylene glycol (DHLA-PEG-OMe) ligand; see Supporting Information Figure S-1 for the structure. The 605 nm streptavidin-functionalized QDs were obtained from Invitrogen (Carlsbad, CA). These CdSe/ZnS QDs are assumed to be made soluble with a proprietary amphiphilic block copolymer coating and further chemically functionalized with an average of between ~5 and 10 streptavidin/QD (www.Invitrogen.com).

DNA Sequences and Chemoselective Ligation to Modified Peptides. DNA sequences were purchased from Operon Biotechnologies, Inc. (Huntsville, AL) (see Figure 1A). Contiguous backbone DNA sequences were obtained with the 3′ end modified as either a free amine or a biotin. Individual segments A−D were obtained dye-labeled with either Cy3 or Cy5 at the 5′ end. Identical unlabeled spacer (sp) A−D sequences were also purchased. 3′-Aminated backbone DNA was covalently linked to the 2-hydrazinonicotinoyl (HYNIC)-modified $(His)_6$-peptide using aniline-catalyzed chemoselective ligation as previously described.[22,31] The peptide sequence is given in Figure 1B. For this, aldehyde-modified DNA sequences were obtained by reacting ~0.45 mM amine-terminated DNA in 1× phosphate buffered saline pH 7.4 (PBS, 137 mM NaCl, 10 mM phosphate, 2.7 mM KCl) with 9.09 mM *p*-formylbenzoic acid-*N*-hydroxysuccinimide ester (Sigma-Aldrich, St. Louis, MO, 100 mM stock solution in dimethyl sulfoxide) at room temperature for 16−18 h. Aldehyde-modified DNA was purified using PD-10 desalting columns (GE Healthcare) and concentrated in a speed vacuum. Concentrations were determined using the DNA absorbance ε_{260nm} of 379 051 M^{-1} cm^{-1} on an Agilent Technologies 8453 UV−visible spectrophotometer (Santa Clara, CA). The final peptido-DNA ligate was produced in the next step by reacting HYNIC-modified $(His)_6$-peptide (1 mM in 10% DMSO/0.1 M ammonium acetate, NH_4OAc, pH 5.5) with aldehyde-modified DNA (2 mM) in the presence of 100 mM aniline at room temperature overnight. The peptide−DNA conjugate was purified using Ni-NTA media (Qiagen, Valencia CA), desalted on an oligonucleotide purification cartridge (Applied Biosystems, Foster City, CA), quantitated using both the DNA and conjugated hydrazone bond absorption (ε_{354} = 29 000 M^{-1} cm^{-1}), dried in a speed vacuum, and stored at −20 °C until needed as described in detail in ref 54.

DNA Hybridization and Assembly to Quantum Dots. For each of the constructs assembled, aliquots of the biotin-labeled backbone, $(His)_6$-peptide-labeled backbone, or the amine-modified backbone DNA were combined in prescribed molar ratios with aliquots of the dye-labeled or unlabeled segments so that one of each of the five parts—the unique backbone along with complementary segments A, B, C, and D (either dye-labeled or as unlabeled sp)—were all present in equimolar concentrations. Construct 1 consists of DNA with no QDs present and utilized Cy3- and Cy5-labeled DNA as donor and acceptor, respectively; 100 pmol of Cy3-labeled donor DNA was assembled on the backbone DNA with varying amounts of 0, 10, 20, 30, 40, 50, 60, 70, 80, 90, 100, and 110 pmol of Cy5-labeled DNA acceptor segments. For each position/ratio of dye acceptor-labeled DNA tested, the total amount of each DNA segment (labeled plus sp) relative to backbone was kept constant by adjustment with unlabeled sp strands. Alternate versions moved the position of the Cy5 label from position B to C and then D. Only one dye-labeled strand/position per construct was interrogated per experiment, but the DNA was always kept in a double-stranded conformation with equimolar sp segments. The DNA was diluted in 1× PBS to a total volume of 100 μL in a 0.5 mL tube for hybridization. Construct 2 (530 nm QD donors, peptide-labeled backbone, and Cy3-labeled DNA acceptors) and construct 3 (605 nm streptavidin QD donors, biotin-labeled backbone, and Cy5-labeled DNA acceptors) used equimolar concentrations of the DNA for the hybridization but adjusted the final hybridized DNA to QD concentrations to alter the relative donor/acceptor ratios. Hybridization was achieved by placing the tubes with DNA in a water bath preheated to 100 °C which was subsequently allowed to cool to 25 °C ambiently (~45 min). For the constructs using QDs, attachment was performed posthybridization in a separate reaction. Twenty picomoles of 530 nm QD solution was mixed with 0, 10, 20, 40, 60, 80, 120, 160, and 200 pmol of the $(His)_6$-peptide double-stranded DNA (dsDNA) and 1× PBS to a final QD concentration of 0.2 μM in 100 μL total volume. The reaction was left for 1 h at room temperature before measurement; 2.5 pmol of 605 nm streptavidin QD donor was mixed with 0, 2.5, 5, 10, 20, 30, 37.5, 50, 57.5, 75, 82.5, and 100 pmol of the biotin-labeled dsDNA and 1× PBS to a final QD concentration of 0.025 μM in 100 μL total volume. The reaction was left overnight at 4 °C before measurement. The difference in concentrations between 530 and 605 nm streptavidin QD donor used in assays is attributable to the 3.5× higher quantum yield of the latter (0.2 *vs* 0.7, respectively).

Data Collection and Förster Resonance Energy Transfer Analysis. Steady-state fluorescence spectra from solutions of dye-labeled DNA and QD−DNA bioconjugates were collected on a Tecan Safire Dual Monochromator Multifunction Microtiter Plate Reader (Tecan, Research Triangle Park, NC) using 520 nm excitation for Cy3 donors and 300 nm for QD donors. For analysis, the direct excitation contribution to each of the acceptors was estimated by assaying control samples prepared in the same manner with either a spacer in place of the dye-labeled DNA donor or the QD omitted from the assembly. These control spectra were utilized to deconvolve the composite spectra into separate donor- and acceptor-sensitized components where appropriate for subsequent analysis. For each QD− or dye−dye donor−acceptor pair, the Förster distance R_0 corresponding to a donor−acceptor separation resulting in 50% energy transfer efficiency was calculated using the expression[32]

$$R_0 = 9.78 \times 10^3[\kappa^2 \check{n}^{-4} Q_D J(\lambda)]^{1/6} \quad (1)$$

where $\check{n}$ is the refractive index of the medium, Q_D is the PL quantum yield (QY) of the donor, $J(\lambda)$ is the spectral overlap integral, and κ^2 is the dipole orientation factor. We use a $\kappa^2 = 2/3$ value shown to be appropriate for the random dipole orientations found within these heterogeneous self-assembled configurations.[11,46,55] This equation is appropriate for units of R_0 in angstroms and $J(\lambda)$ in $cm^3\ M^{-1}$. Average energy transfer efficiency E was extracted for each set of donor−acceptor conjugates using the expression

$$E = \frac{(F_D - F_{DA})}{F_D} \quad (2)$$

where F_D and F_{DA} are, respectively, the fluorescence intensities of the donor alone and donor in the presence of acceptor(s). Where appropriate, we assume that each construct exhibits a centrosymmetric distribution of acceptors characterized by constant average center-to-center separation distances.[46,55] Energy transfer efficiency data can then be fit to the expression[55]

$$E = \frac{nR_0^6}{nR_0^6 + r^6} \quad (3)$$

where n is the average number of acceptors per donor. For QD conjugates specifically demonstrating high FRET E with small numbers of acceptors (40−50% at $n \leq 2$), the heterogeneity in conjugate valence is accounted for by using a Poisson distribution function, $p(N,n)$, during the fitting of the efficiency data:[56]

$$E = \sum_n p(N,n)E(n) \text{ and } p(N,n) = N^n \frac{e^{-N}}{n!} \quad (4)$$

where n designates the exact numbers of acceptors (valence) for conjugates with a nominal average valence of N.

Structural Modeling. Computational simulations of the QD−DNA architectures progressed in several phases: (1) construction of a double-stranded DNA segment of 40 base pairs; (2) appending a biotinylated linker or peptide HYNIC linker to the DNA; (3) docking the biotinylated DNA to streptavidin; and (4) placing the streptavidin on the surface of a QD or attaching the $(His)_6$ portion of the peptide onto the QD surface. This was followed by making the required measurements along with adjustments to torsional angles and final rendering of images. Starting with PDB entry 142D,[57] which is a 13 base pair sequence of DNA from the HIV-1 genome, a 41 base pair model was constructed by aligning residues at the end of the chain with another copy of the same model until the desired chain length was achieved. This sequence was utilized as crystallographic coordinates of the actual sequences used in the experiments are not available. The relative interchangeability of dsDNA structures and the maintenance of persistence length allow us to use it as a representative sequence and to estimate distances with some fidelity for our purposes. The sequence of a single strand is 5′-ACAGCTTATA-ATCGATCACG-TCAGCTTATC-ATCGATCACG-T-3′ (plus complement for the double-stranded model). The biotinylated linker (Figure 1A) was constructed using Chem-3D Ultra 11.0 and energy minimized using the MM2 module. The linkers (biotin or peptide) were then attached to the 3′ end of the previously constructed DNA model. Owing to the nature of the binding site in streptavidin (*i.e.*, the site is buried deep within the protein), an extended conformation was selected for the linker in order to avoid unfavorable contacts between streptavidin, the linker, and the attached DNA models. The biotinylated DNA was docked with the avidin structure from PDB entry 1AVD.[58] The biotin in that complex acted as a guide allowing adjustment of torsion angles in the linker to minimize or eliminate unfavorable contacts.

For constructing the QD−peptido−DNA structure shown in Figure 5A, crystallographic data on Cy3 dye was not available, thus a model for the three-dimensional conformation of Cy3-maleimide that was previously constructed using Chem-3D Ultra 8.0 was utilized.[45] Low energy conformers were located using the MM2 molecular dynamics module within Chem-3D Ultra for energy minimization. Energies of these conformers were found to range from 17.9 to 23.0 kcal/mol. A conformer was selected that had the maleimide oriented such that it could interact with a cysteine side chain on a peptide to form a covalent bond. The maximum distance from the expected linkage point to the fluorescent dye center was determined to be ~14.6 Å. This distance was used as the radius of spheres located at four points along the DNA to indicate the maximum range of possible locations of dye position given full freedom of rotation, although actual locations are expected to be closer to the DNA. The peptide−DNA HYNIC covalent bond was also constructed in Chem-3D Ultra 11.0 and energy minimized using the MM2 module. The full peptide−DNA construct was then attached to the QD surface and torsion angles adjusted.[46] The extended length of the DHLA-PEG-OMe ligand on the QD surface was estimated by energy minimization.

For the QD-streptavidin−biotinylated-DNA structure shown in Figure 5B, the radius of the QD with surface polymer coating was conservatively estimated at 75 Å based on manufacturer specifications. The streptavidin molecule is directly coupled to the QD surface polymer (also based on specifications) and was docked to the biotinylated DNA using the biotin linker shown in Figure 1A. Two extremes for the orientation of the biotin−DNA complex relative to the QD surface were examined: the DNA chain fully extended away from the QD surface and the DNA chain tangential to the QD surface (see also Supporting Information Figure S-6). These were obtained by simply rotating the streptavidin conformation relative to the QD. Distance from the QD center to bases 1, 11, 21, and 31 of the DNA (attachment points for fluorescent dye) were measured within Chimera[59] and were found to be 128, 156, 186, and 215 Å for the extended orientation and 98, 93, 90, and 105 Å for the tangential orientation. The actual location of the fluorophore can vary by a maximum of ±14.6 Å from these distances after excluding conformations that result in unfavorable contacts as described above. For predicting donor−acceptor separation distances, we utilize a more conservative, energetically favorable estimate of 10 Å for the dye's rotational freedom.

Acknowledgment. The authors acknowledge the CB Directorate/Physical S&T Division (DTRA), ONR, NRL, and the NRL-NSI for financial support. K.B. and D.P. acknowledge ASEE fellowships through NRL. J.B.B.-C acknowledges a Marie Curie IOF. UCSF Chimera package from the Resource for Biocomputing, Visualization, and Informatics at the University of California, San Francisco was also utilized (supported by NIH P41 RR-01081).

Supporting Information Available: Results of modeling the DNA with and without nicks in its structure, DHLA-PEG-OMe and dye structures, comparison plots of FRET *E*/FRET *E* corrected where appropriate along with acceptor sensitization for selected configurations, and alternate models of single DNA 605 nm QD−streptavidin. This material is available free of charge *via* the Internet at http://pubs.acs.org.

REFERENCES AND NOTES

1. Gill, R.; Zayats, M.; Willner, I. Semiconductor Quantum Dots for Bioanalysis. *Angew. Chem., Int. Ed.* **2008**, *47*, 7602–7625.
2. Pumera, M.; Sanchez, S.; Ichinose, I.; Tang, J. Electrochemical Nanobiosensors. *Sens. Actuators. B* **2007**, *123*, 1195–1205.
3. Cheon, J.; Lee, J. H. Synergistically Integrated Nanoparticles as Multimodal Probes for Nanobiotechnology. *Acc. Chem. Res.* **2008**, *41*, 1630–1640.
4. Medintz, I. Universal Tools for Biomolecular Attachment to Surfaces. *Nat. Mater.* **2006**, *5*, 842.
5. Aubin-Tam, M. E.; Hamad-Schifferli, K. Structure and Function of Nanoparticle-Protein Conjugates. *Biomed. Mater.* **2008**, *3*, 034001.
6. Hermanson, G. T. *Bioconjugate Techniques*, 2nd ed.; Academic Press: San Diego, CA, 2008.
7. Diamandis, E. P.; Christopoulos, T. K. The Biotin−(Strept)Avidin System: Principles and Applications in Biotechnology. *Clin. Chem.* **1991**, *37*, 625–636.
8. Zhao, Z. D.; Yuan, W. Z.; Gu, S. Y.; Ren, T. B.; Ren, J. "Click Chemistry" and Its Growing Applications in Biomedical Field. *Prog. Chem.* **2010**, *22*, 417–426.
9. Mamidyala, S. K.; Finn, M. G. *In Situ* Click Chemistry: Probing the Binding Landscapes of Biological Molecules. *Chem. Soc. Rev.* **2010**, *39*, 1252–1261.
10. Tiefenbrunn, T. K.; Dawson, P. E. Chemoselective Ligation Techniques: Modern Applications of Time-Honored Chemistry. *Biopolymers* **2010**, *94*, 95–106.
11. Medintz, I. L.; Mattoussi, H. Quantum Dot-Based Resonance Energy Transfer and Its Growing Application in Biology. *Phys. Chem. Chem. Phys.* **2009**, *11*, 17–45.
12. Algar, W. R.; Massey, M.; Krull, U. J. The Application of Quantum Dots, Gold Nanoparticles and Molecular Switches to Optical Nucleic-Acid Diagnostics. *Trac-Trends Anal. Chem.* **2009**, *28*, 292–306.
13. Biju, V.; Itoh, T.; Ishikawa, M. Delivering Quantum Dots to Cells: Bioconjugated Quantum Dots for Targeted and Nonspecific Extracellular and Intracellular Imaging. *Chem. Soc. Rev.* **2010**, *39*, 3031–3056.
14. Delehanty, J. B.; Bradburne, C. E.; Boeneman, K.; Susumu, K.; Farrell, D.; Mei, B. C.; Blanco-Canosa, J. B.; Dawson, G.; Dawson, P. E.; Mattoussi, H.; Medintz, I. L. Delivering Quantum Dot−Peptide Bioconjugates to the Cellular Cytosol: Escaping from the Endolysosomal System. *Integr. Biol.* **2010**, *2*, 265–277.
15. Geißler, D.; Charbonnière, L. J.; Ziessel, R. F.; Butlin, N. G.; Löhmannsröben, H. G.; Hildebrandt, N. Quantum Dot Biosensors for Ultrasensitive Multiplexed Diagnostics. *Angew. Chem., Int. Ed.* **2010**, *49*, 1396–1401.
16. Morgner, F.; Geissler, D.; Stufler, S.; Butlin, N. G.; Löhmannsröben, H. G.; Hildebrandt, N. A Quantum-Dot-Based Molecular Ruler for Multiplexed Optical Analysis. *Angew. Chem., Int. Ed.* **2010**, doi: *49*, 7570−7574.
17. Medintz, I.; Uyeda, H.; Goldman, E.; Mattoussi, H. Quantum Dot Bioconjugates for Imaging, Labeling and Sensing. *Nat. Mater.* **2005**, *4*, 435–446.
18. Klostranec, J. M.; Chan, W. C. W. Quantum Dots in Biological and Biomedical Research: Recent Progress and Present Challenges. *Adv. Mater.* **2006**, *18*, 1953–1964.
19. Michalet, X.; Pinaud, F. F.; Bentolila, L. A.; Tsay, J. M.; Doose, S.; Li, J. J.; Sundaresan, G.; Wu, A. M.; Gambhir, S. S.; Weiss, S. Quantum Dots for Live Cells, *In Vivo* Imaging, and Diagnostics. *Science* **2005**, *307*, 538–544.
20. Sapsford, K. E.; Pons, T.; Medintz, I. L.; Higashiya, S.; Brunel, F. M.; Dawson, P. E.; Mattoussi, H. Kinetics of Metal-Affinity Driven Self-Assembly between Proteins or Peptides and CdSe−ZnS Quantum Dots. *J. Phys. Chem. C* **2007**, *111*, 11528–11538.
21. Berti, L.; D'Agostino, P. S.; Boeneman, K.; Medintz, I. L. Improved Peptidyl Linkers for Self-Assembling Semiconductor Quantum Dot Bioconjugates. *Nano Res.* **2009**, *2*, 121–129.
22. Prashun, D. E.; Blanco-Canosa, J. B.; Vora, G. J.; Delehanty, J. B.; Susumu, K.; Mei, B. C.; Dawson, P. E.; Medintz, I. L. Combining Chemoselective Ligation with Polyhistidine-Driven Self-Assembly for the Modular Display of Biomolecules on Quantum Dots. *ACS Nano* **2010**, *4*, 267–278.
23. Ueda, E. K. M.; Gout, P. W.; Morganti, L. Current and Prospective Applications of Metal Ion-Protein Binding. *J. Chromatogr. A* **2003**, *988*, 1–23.
24. Ohya, Y.; Yabuki, K.; Hashimoto, M.; Nakajima, A.; Ouchi, T. Multistep Fluorescence Resonance Energy Transfer in Sequential Chromophore Array Constructed on Oligo-DNA Assemblies. *Bioconjugate Chem.* **2003**, *14*, 1057–1066.
25. Protozanova, E.; Yakovchuk, P.; Frank-Kamenetskii, M. D. Stacked-Unstacked Equilibrium at the Nick Site of DNA. *J. Mol. Biol.* **2004**, *342*, 775–785.
26. Dennis, A. M.; Bao, G. Quantum Dot−Fluorescent Protein Pairs as Novel Fluorescence Resonance Energy Transfer Probes. *Nano Lett.* **2008**, *8*, 1439–1445.
27. Dif, A.; Henry, E.; Artzner, F.; Baudy-Floch, M.; Schmutz, M.; Dahan, M.; Marchi-Artzner, V. Interaction between Water-Soluble Peptidic CdSe/ZnS Nanocrystals and Membranes: Formation of Hybrid Vesicles and Condensed Lamellar Phases. *J. Am. Chem. Soc.* **2008**, *130*, 8289–8296.
28. Liu, W.; Howarth, M.; Greytak, A. B.; Zheng, Y.; Nocera, D. G.; Ting, A. Y.; Bawendi, M. G. Compact Biocompatible Quantum Dots Functionalized for Cellular Imaging. *J. Am. Chem. Soc.* **2008**, *130*, 1274–1284.
29. Boeneman, K.; Delehanty, J. B.; Susumu, K.; Stewart, M. H.; Medintz, I. L. Intracellular Bioconjugation of Targeted Proteins with Semiconductor Quantum Dots. *J. Am. Chem. Soc.* **2010**, *132*, 5975–5977.
30. Medintz, I. L.; Berti, L.; Pons, T.; Grimes, A. F.; English, D. S.; Alessandrini, A.; Facci, P.; Mattoussi, H. A Reactive Peptidic Linker for Self-Assembling Hybrid Quantum Dot−DNA Bioconjugates. *Nano Lett.* **2007**, *7*, 1741–1748.
31. Dirksen, A.; Dawson, P. E. Rapid Oxime and Hydrazone Ligations with Aromatic Aldehydes for Biomolecular Labeling. *Bioconjugate Chem.* **2008**, *19*, 2543–2548.
32. Lakowicz, J. R. *Principles of Fluorescence Spectroscopy*, 3rd ed.; Springer: New York, 2006.
33. Dabbousi, B. O.; Rodriguez-Viejo, J.; Mikulec, F. V.; Heine, J. R.; Mattoussi, H.; Ober, R.; Jensen, K. F.; Bawendi, M. G. (CdSe)ZnS Core−Shell Quantum Dots: Synthesis and Optical and Structural Characterization of a Size Series of Highly Luminescent Materials. *J. Phys. Chem. B* **1997**, *101*, 9463–9475.
34. Zhang, C. Y.; Johnson, L. W. Quantum Dot-Based Fluorescence Resonance Energy Transfer with Improved FRET Efficiency in Capillary Flows. *Anal. Chem.* **2006**, *78*, 5532–5537.
35. Zhang, C. Y.; Johnson, L. W. Quantum-Dot-Based Nanosensor for RRE IIB RNA-Rev Peptide Interaction Assay. *J. Am. Chem. Soc.* **2006**, *128*, 5324–5325.
36. Kim, J. H.; Chaudhary, S.; Ozkan, M. Multicolour Hybrid Nanoprobes of Molecular Beacon Conjugated Quantum Dots: FRET and Gel Electrophoresis Assisted Target DNA Detection. *Nanotechnology* **2007**, *18*, 195105.
37. Cady, C. N.; Strickland, A. D.; Batt, C. A. Optimized Linkage and Quenching Strategies for Quantum Dot Molecular Beacons. *Mol. Cell. Probes* **2007**, *21*, 116–124.
38. Hohng, S.; Ha, T. Single-Molecule Quantum-Dot Fluorescence Resonance Energy Transfer. *ChemPhysChem* **2005**, *6*, 956–960.
39. Zhang, C.-Y.; Johnson, L. W. Microfluidic Control of Fluorescence Resonance Energy Transfer: Breaking the FRET Limit. *Angew. Chem., Int. Ed.* **2007**, *46*, 3482–3485.
40. Zhang, C. Y.; Yeh, H. C.; Kuroki, M. T.; Wang, T. H. Single-Quantum-Dot-Based DNA Nanosensor. *Nat. Mater.* **2005**, *4*, 826–831.
41. Levy, M.; Cater, S. F.; Ellington, A. D. Quantum-Dot Aptamer Beacons for the Detection of Proteins. *ChemBioChem* **2005**, *6*, 2163–2166.
42. Zhang, C. Y.; Hu, J. Single Quantum Dot-Based Nanosensor for Multiple DNA Detection. *Anal. Chem.* **2010**, *82*, 1921–1927.
43. Chen, Z.; Li, G.; Zhang, L.; Jiang, J. F.; Li, Z.; Peng, Z. H.;

Deng, L. A New Method for the Detection of ATP Using a Quantum-Dot-Tagged Aptamer. *Anal. Bioanal. Chem.* **2008**, *392*, 1185–1188.
44. Suzuki, M.; Husimi, Y.; Komatsu, H.; Suzuki, K.; Douglas, K. T. Quantum Dot FRET Biosensors that Respond to pH, to Proteolytic or Nucleolytic Cleavage, to DNA Synthesis, or to a Multiplexing Combination. *J. Am. Chem. Soc.* **2008**, *130*, 5720–5725.
45. Medintz, I. L.; Konnert, J. H.; Clapp, A. R.; Stanish, I.; Twigg, M. E.; Mattoussi, H.; Mauro, J. M.; Deschamps, J. R. A Fluorescence Resonance Energy Transfer Derived Structure of a Quantum Dot−Protein Bioconjugate Nanoassembly. *Proc. Natl. Acad. Sci. U.S.A.* **2004**, *101*, 9612–9617.
46. Medintz, I. L.; Clapp, A. R.; Brunel, F. M.; Tiefenbrunn, T.; Uyeda, H. T.; Chang, E. L.; Deschamps, J. R.; Dawson, P. E.; Mattoussi, H. Proteolytic Activity Monitored by Fluorescence Resonance Energy Transfer through Quantum-Dot−Peptide Conjugates. *Nat. Mater.* **2006**, *5*, 581–589.
47. Zhou, M.; Ghosh, I. Quantum Dots and Peptides: A Bright Future Together. *Biopolymers* **2007**, *88*, 325–339.
48. Xu, C. J.; Xing, B. G.; Rao, H. H. A Self-Assembled Quantum Dot Probe for Detecting β-Lactamase Activity. *Biochem. Biophys. Res. Commun.* **2006**, *344*, 931–935.
49. Algar, W. R.; Krull, U. J. New Opportunities in Multiplexed Optical Bioanalyses Using Quantum Dots and Donor-Acceptor Interactions. *Anal. Bioanal. Chem.* **2010**, *398*, 2439−2449.
50. McLaurin, E. J.; Greytak, A. B.; Bawendi, M. G.; Nocera, D. G. Two-Photon Absorbing Nanocrystal Sensors for Ratiometric Detection of Oxygen. *J. Am. Chem. Soc.* **2009**, *131*, 12994–13001.
51. Daniel, M. C.; Astruc, D. Gold Nanoparticles: Assembly, Supramolecular Chemistry, Quantum-Size-Related Properties, and Applications toward Biology, Catalysis, and Nanotechnology. *Chem. Rev.* **2004**, *104*, 293–346.
52. Burda, C.; Chen, X. B.; Narayanan, R.; El-Sayed, M. A. Chemistry and Properties of Nanocrystals of Different Shapes. *Chem. Rev.* **2005**, *105*, 1025–1102.
53. Peng, Z. A.; Peng, X. Formation of High-Quality CdTe, CdSe, and CdS Nanocrystals Using CdO as Precursor. *J. Am. Chem. Soc.* **2001**, *123*, 183–184.
54. Sapsford, K. E.; Farrell, D.; Sun, S.; Rasooly, A.; Mattoussi, H.; Medintz, I. L. Monitoring of Enzymatic Proteolysis on a Electroluminescent-CCD Microchip Platform Using Quantum Dot−Peptide Substrates. *Sens. Actuators B* **2009**, *139*, 13–21.
55. Clapp, A. R.; Medintz, I. L.; Mauro, J. M.; Fisher, B. R.; Bawendi, M. G.; Mattoussi, H. Fluorescence Resonance Energy Transfer between Quantum Dot Donors and Dye-Labeled Protein Acceptors. *J. Am. Chem. Soc.* **2004**, *126*, 301–310.
56. Pons, T.; Medintz, I. L.; Wang, X.; English, D. S.; Mattoussi, H. Solution-Phase Single Quantum Dot Fluorescence Resonant Energy Transfer Sensing. *J. Am. Chem. Soc.* **2006**, *128*, 15324–15331.
57. Mujeeb, A.; Kerwin, S. M.; Kenyon, G. L.; James, T. L. Solution Structure of a Conserved DNA Sequence from the HIV-1 Genome: Restrained Molecular Dynamics Simulation with Distance and Torsion Angle Restraints Derived from Two-Dimensional NMR. *Biochemistry* **1993**, *32*, 13419–13431.
58. Pugliese, L.; Coda, A.; Malcovati, M.; Bolognesi, M. Three-Dimensional Structure of the Tetragonal Crystal Form of Egg-White Avidin in Its Functional Complex with Biotin at 2.7 Å Resolution. *J. Mol. Biol.* **1993**, *231*, 698–710.
59. Pettersen, E. F.; Goddard, T. D.; Huang, C. C.; Couch, G. S.; Greenblatt, D. M.; Meng, E. C.; Ferrin, T. E. UCSF Chimera—A Visualization System for Exploratory Research and Analysis. *J. Comput. Chem.* **2004**, *25*, 1605–1612.